7
Polystyrene to Graphitic Carbon for Supercapacitors

(Cited work: Urgunde et al., ACS Appl. Electron. Mater. 2020, 2, 3178−3186)

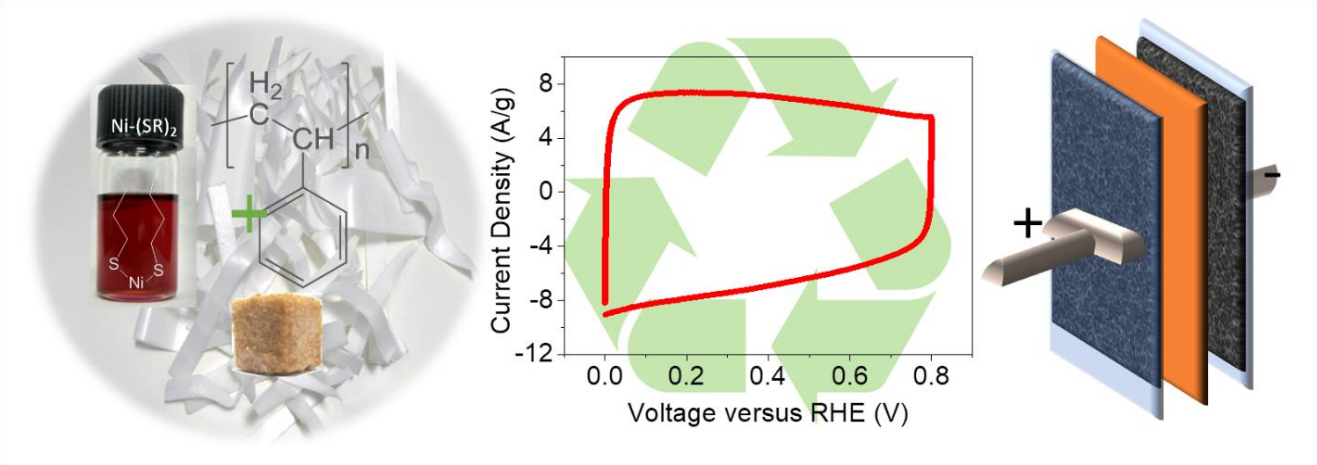

7.1 Introduction

Polystyrene is one of the first synthetic polymer that was observed in the euphotic zone in oceans during the 1970s and is still observed today. Ten crore tons of polystyrene is manufactured per year globally as it is used in a vast number of products, which includes containers for food, protective packaging, and materials for building as composites. Although there is the widespread use of polystyrene-based goods, polystyrene is poorly constrained for its widespread and management. [Gutiérrez et al., 2012] The lack of waste management worldwide makes it an alarming situation because of polystyrene's hazardous nature and its decomposed components (Figure 7.1). Styrene particles leached into the aqueous ecosystems rapidly get absorbed in the living beings, ultimately concentrating on the food chain.[Aciu et al., 2015]

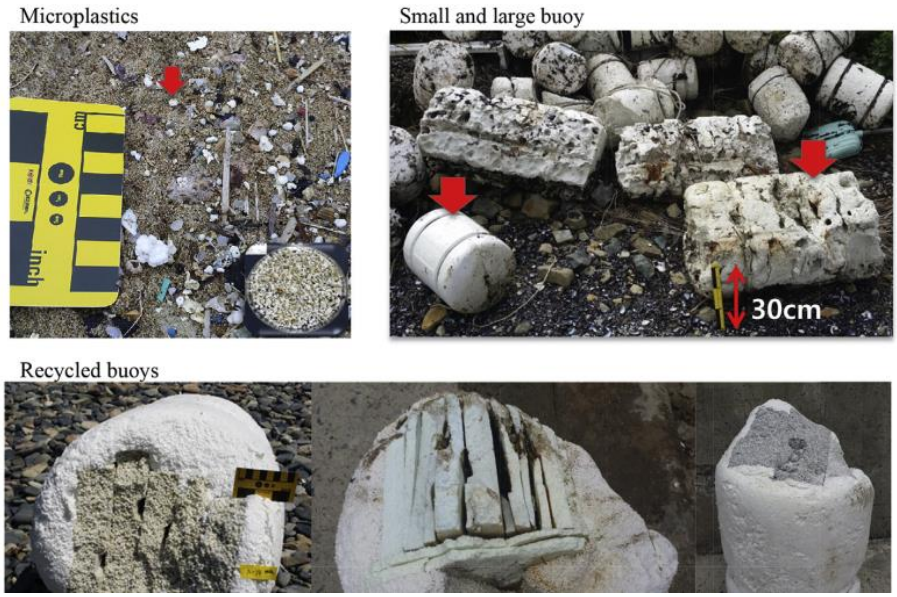

Figure 7.1: Expanded polystyrene as pollutant. Figures are adapted from reference [Jang et al., 2017]

Therefore, it is highly essential to develop a simple strategy for the conversion of polystyrene or any other waste carbon source to graphitic carbon at a competitive price without sacrificing the

performance for it to become a technological solution. Herein, a large-scale synthesis of microporous graphitic carbon derived from waste polystyrene and porous sugar as a carbon source is demonstrated by pyrolysis in hydrogen atmosphere , which was subsequently used to prepare supercapacitor electrodes. Ni as a catalyst has been vastly used in literature for the growth of 2D crystalline carbon materials because of notable advantages in comparison to other metals. Ni has higher carbon solubility and drastically reduces the processing temperature and time without any special need for high-vacuum conditions for carbon growth. It allows graphene growth and promotes better crystallinity.[Kim et al., 2011; Kumar et al., 2019; Wang et al., 2011; Yoon et al., 2012] Ni is usually deposited by physical methods that restrict the surface to planar geometries. However, in this work, Ni-complex ink impregnated in polystyrene is used directly as a catalyst for carbon growth for obtaining conducting and graphitic carbon. The carbon electrodes prepared in this study are demonstrated to possess excellent specific capacitance at faster rates and long term cyclic stability.

7.2 Objectives of the Work

The objectives of this work are as follows:

1. To synthesize template-free graphitic carbon material from waste polystyrene using highly solution processed Ni-butanethiolate catalyst ink.
2. To optimize the synthetic conditions for high surface area graphitized carbon with excellent electrochemical properties
3. To fabricate high performance EDLC from waste polystyrene derived carbon material.

7.3 Experimental

7.3.1 Synthesis of Nickel butanethiolate Catalyst

The Ni-BT precursor was synthesized using general two-step process, detailed in Chapter 2, section 2.4.2.

7.3.2 Graphitic Carbon Conversion

The raw polystyrene beads were purchased from Nova Chemicals (Mumbai). Waste polystyrene foam plates were cut into pieces of irregular shapes (0.3-1 cm size) as carbon source. The waste pieces were washed in dilute HCl and water to remove surface contaminants and dissolved in chloroform (0.25 g/mL) to make a solution for further use. The Ni-butanethiolate complex was added to the polystyrene solution before casting it in regular sugar cubes (Daurala Sugar Works) to form the composite. The weight of polystyrene, sugar cube, and Ni butanethiolate catalyst were taken in the ratio 1:3:0.002 (grams). The polymer and sugar composites were made by soaking sugar cube into a polystyrene solution with and without Ni-butanethiolate complex as a catalyst. The sugar cubes were left to dry until the chloroform is evaporated. The sugar-polystyrene composite was then pyrolyzed in a muffle furnace with a gravimetric scale (Nabertherm-B400) under 5% hydrogen in nitrogen gas atmosphere. The temperature of the furnace was ramped from room temperature to the desired temperature (800 °C) at 20 °C/min for 1 h, followed by cooling to room temperature. The pyrolysis temperature was optimized based on Raman analysis. The residue yielded ~15% carbon by weight. A further hydrogenation of pyrolysed carbon was performed by annealing at 1000 °C for 2 h for graphitization.

7.3.3 Material Characterization

X-ray diffraction (XRD) patterns were recorded from 2° to 70° at a scan rate of 0.02 °/s using Rigaku Ultima IV with Cu Kα (λ=1.5406 Å). Raman spectra of the carbon samples were recorded with Renishaw, UK (523 nm laser diode and the spectra were deconvoluted using Fityk 1.3.1 (open source) software with Lorentzian and Gaussian curve fitting for analysis. The powdered carbon samples were dispersed in IPA and sonicated for 15 mins. The solution was drop coated on the copper grid for TEM analysis. HRTEM and ED pattern was recorded using Talos 2000S G2 FEG, and images were analyzed using Gatan GMS 3 software (open source). Thermogravimetric analysis (TGA) of samples (~4 mg) was performed at a rate of 10 °C/min in N_2 atmosphere by using Simultaneous Thermal Analyzer, Perkin Elmer. All the electrochemical measurements were performed on CH workstation model CHI660E. Fourier Transform Infrared spectroscopy (FTIR) was done using Bruker Vertex 70 V+PMA50 spectrometer in the range of 600 to 4000 cm^{-1}. The carbon pellets were prepared with standard activated KBr (analytical grade). Brunauer–Emmett–Teller (BET) adsorption-desorption isotherms were performed using Quantachrome Autosorb iQ3, and pore size distribution was analyzed by non-local density functional theory (NLDFT). The I-V measurements are performed in two-probe geometry laterally across the graphitic carbon samples taken in the form of a pellet of thickness ~2 mm and diameter 10 mm.

7.3.4 Electrochemical Measurements

The electrochemical measurements in three-electrode geometry were performed in a 3 M KOH solution using Ag/AgCl as a reference electrode and platinum wire as a counter electrode. The Ag/AgCl electrode was refilled with a saturated KCl solution and calibrated for every electrode measurement to ensure the correctness in the results. The working electrode was prepared on a glassy carbon electrode by drop-casting 5 µL dispersion of the carbon material (10 mg) in 750 µL isopropyl alcohol and 80 µL Nafion (CAS: 31175-20-9, Sigma Aldrich). Two-electrode supercapacitor device is assembled in a Swagelok geometry using graphitic carbon coated on carbon cloth as electrodes on either side separated by a Celgard membrane in 3 M KOH solution. Graphitic carbon dispersed in IPA containing 10% Nafion was drop-coated on two electrodes of the same size (~0.2 cm^2), with an optimum loading of 0.28 and 0.30 mg/cm^2 and used in symmetric EDLC device fabrication.Cyclic Voltammetry (CV) measurements were performed at variable scan rates ranging from 10-100 mV/s. Galvanostatic Charge-Discharge (GCD) measurements were performed in a range of applied current density (1- 20 A/g) in the voltage window of 0 to 0.8 V versus RHE. The capacitance, power density and energy density were calculated using the equations in section of chapter 2. Electrochemical Impedance Spectroscopy (EIS) was performed in the frequency range of 0.1 to 10 MHz at 0.8 V versus RHE. The loading was optimized to 0.4 mg/cm^2 with respect to the unit area for maximum gravimetric capacitance. With the increase in graphitic carbon from 0.4 to 1 mg/cm^2, the gravimetric capacitance almost remained constant and decreased upon a further increase in the loading to 2.1 mg/cm^2. CV measurements were performed in the voltage range of 1 to 1.6 V versus RHE corresponding to the redox region for Ni nanoparticles to ensure their negligible contribution of graphitic carbon to charge storage.

7.4 Results and Discussion

7.4.1 Synthesis of Graphitic Carbon and Mechanism

The experimental method adopted for the synthetic conversion process is described in Figure 7.3. Briefly, polystyrene and Ni-butanethiolate in chloroform were dissolved together as a uniform solution and infiltrated in sugar cubes and air-dried to form sugar-polystyrene-catalyst

(SPC) composite, as shown in the first step (Figure 7.2). The composite to graphitic carbon conversion is schematically illustrated in Figure 7.3. Ni-butanethiolate has a lamellar structure and easily dissolves in organic solvents to form Ni ink.[John et al., 2007c] It decomposes sharply at 250 °C, yielding Ni-based nanoparticles in hydrogen atmosphere.[Gupta et al., 2017a].

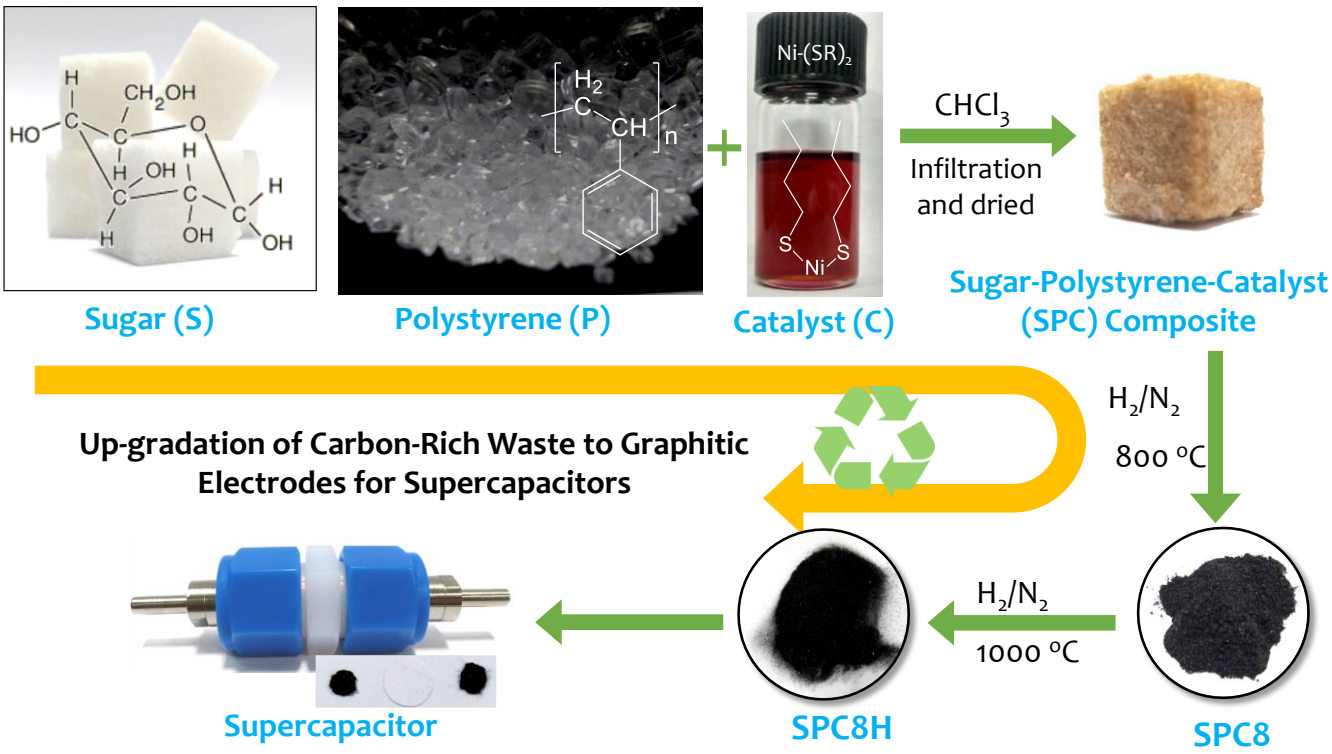

Figure 7.2: Schematic demonstrating steps for conversion of the sugar-polystyrene composite to graphitic carbon in the presence of Ni-butanethiolate ink as a catalyst

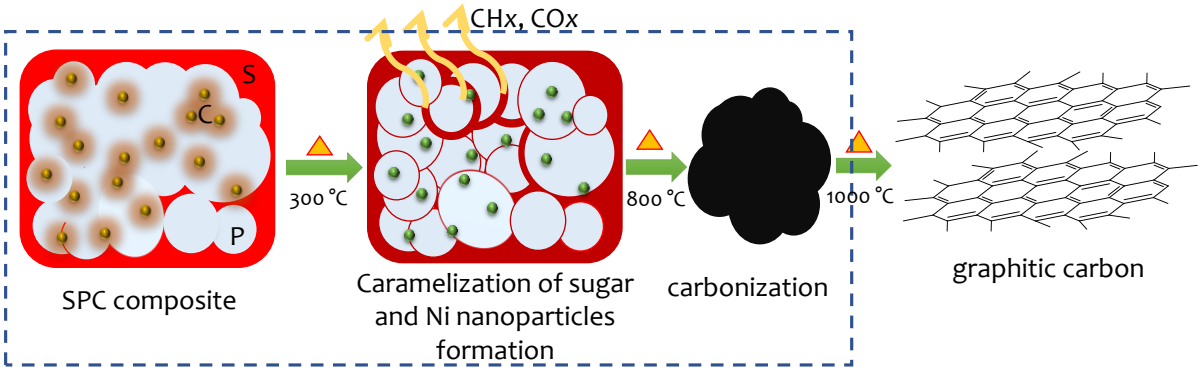

Figure 7.3: Schematic illustration of the mechanism involved in the formation of graphitic carbon.

7.4.2 Material Characterization of the Synthesized Graphitic Carbon

The chemical nature of Ni in the graphitic carbon is confirmed to be Ni(0) from XRD analysis of Ni catalyst obtained from thermolysis of Ni butanethiolate in 5% hydrogen atmosphere (Figure 7.4).

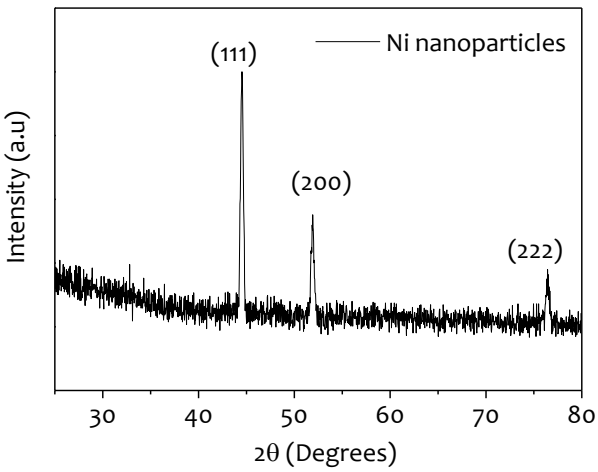

Figure 7.4: XRD pattern of Ni catalyst obtained from thermolysis of Ni butanethiolate in 5% hydrogen

A known weight of SPC composite was placed in a silica crucible and covered with ceramic cover while heating under optimized conditions to reduce the weight loss and aid in the formation of carbon material. Importantly, the process was carried out without any pressurized conditions.

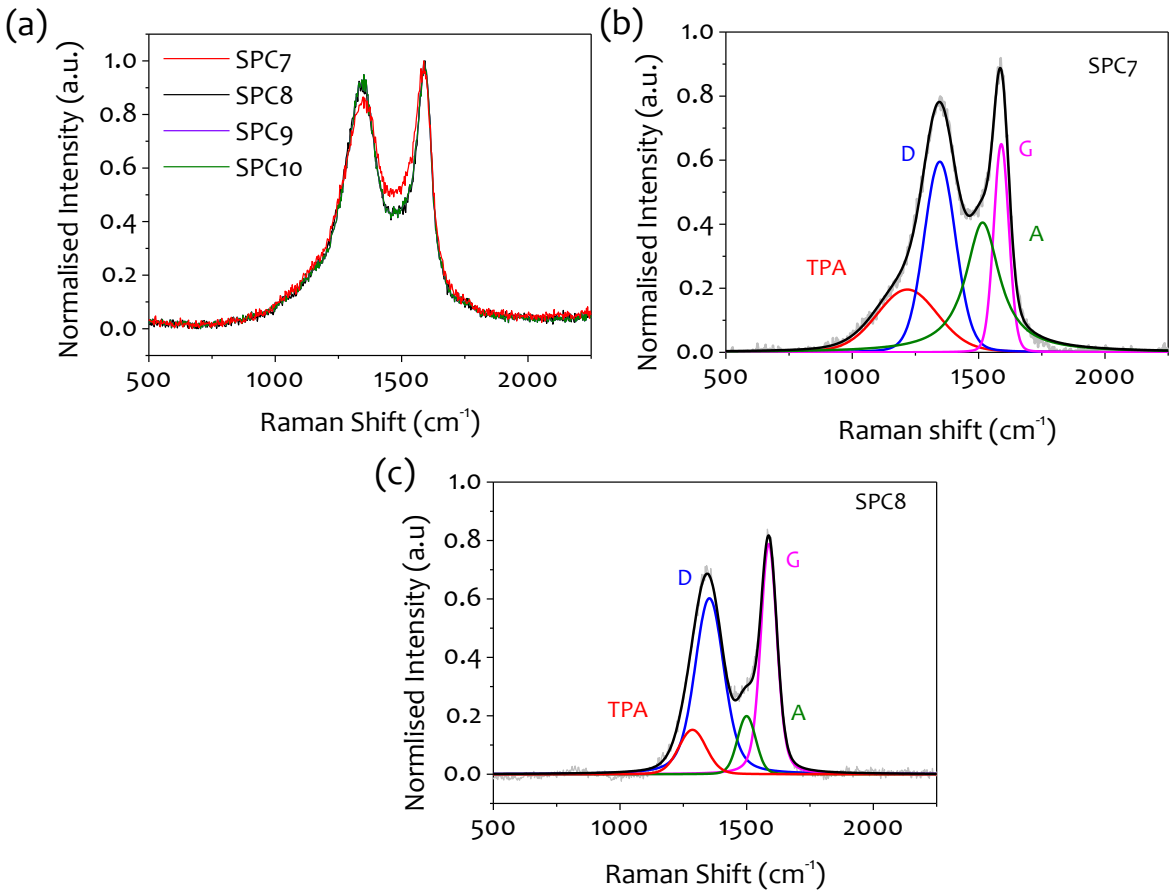

Figure 7.5: (a) Raman spectra of SPC7, SPC8, SPC9, and SPC10. Deconvoluted Raman spectrum of (b) SPC7 (c) SPC8, respectively.

As expected, polystyrene evaporated completely from the crucible at high temperatures. Interestingly, SP and SPC composite yielded highly porous and shiny carbon residues as a product independent of the presence of a catalyst. SPC composite was pyrolyzed at different temperatures of 700 °C, 800 °C, 900 °C, and 1000 °C, and the Raman spectra were analyzed as shown in Figure 7.5. The D and G bands are almost overlapping for SPC8, SPC9, and SPC10 and

differ with SPC7 (Figure 7.5a). The deconvoluted Raman spectra of SPC7 and SPC8 carbon show a decrease in the TPA-structures and A-band in SPC8 compared to SPC7 (Figure 7.5b and c). Raman spectra for the samples annealed above 800 °C did not show any changes; thus, 800 °C was found to be an optimum heating temperature. The carbon samples produced at 800 °C with Ni ink as catalysts are labeled as SPC8 and SP8 (without catalyst). Later, SPC8 and SP8 were hydrogen annealed at a high temperature (1000 °C) to improve the graphitization in the presence and absence of catalyst resulting in SPC8H and SP8H carbon, respectively.

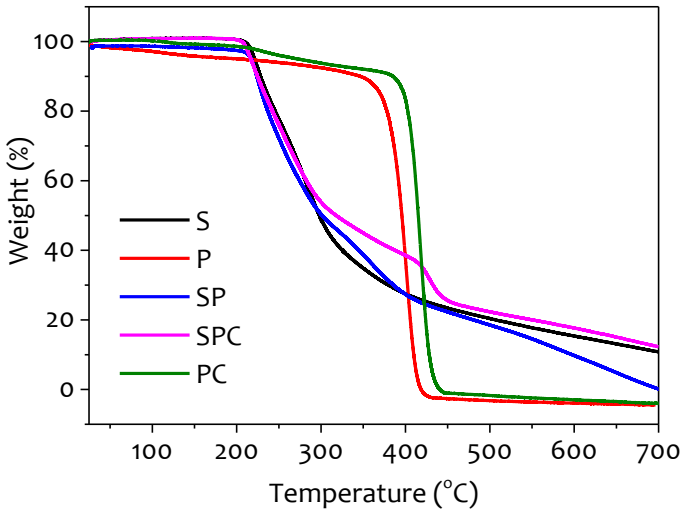

Figure 7.6: Thermogravimetric Analysis (TGA) of sugar (S), polystyrene (P), sugar polymer composite with (SPC) and without catalyst (SP), polymer catalyst (PC) in nitrogen at 10 °C/min.

From thermogravimetric data (Figure 7.6), the exact yield could not be calculated due to differences in the pyrolytic conditions adopted for synthesis; however, it is noted that the decomposition temperature profile depends on the ratio of sugar and catalyst in the polymer. The reaction mechanism is illustrated in Figure 7.3. Briefly, as the SP or SPC composite is heated, firstly, sugar starts decomposing at a temperature of ~211°C. The pyrolytic hydrocarbons from polystyrene get constrained within the carbon shell formed by the caramelization of sugar. Later, polystyrene decomposes at a relatively higher temperature of 400 °C. Interestingly, there is a marked difference in the thermal decomposition profile of SPC composite with respect to SP, indicating the role of catalyst in graphitization of polystyrene trapped in sugar. Since Ni-butanethiolate catalyst is reduced to Ni-based nanoparticles at elevated temperatures (250 °C), the dissolution of hydrocarbons in Ni-based nanoparticles takes place and modifies the decomposition profile. The dissolved carbon recrystallizes forming hexagonal carbon rings, which on further annealing at 1000 °C for 2 h in hydrogen grow into a bigger atomnet with improved crystallinity. Thus, the method presented here poses several key advantages; firstly, on heating, sugars chars and trap the polystyrene, which increases the carbonization and sugar itself acts as a carbon-rich source. Secondly, sugar cube acts as a soft, macroporous-template for holding polystyrene without requiring any hard template. It also eliminates the need for high-pressure autoclave and complicated multistep processes. Lastly, the Ni-butanethiolate ink is used as a catalyst in low quantity, which is rarely the case in solid-state heterogeneous catalysis, and this is made possible due to the excellent dispersion of the Ni-ink in the composite form.

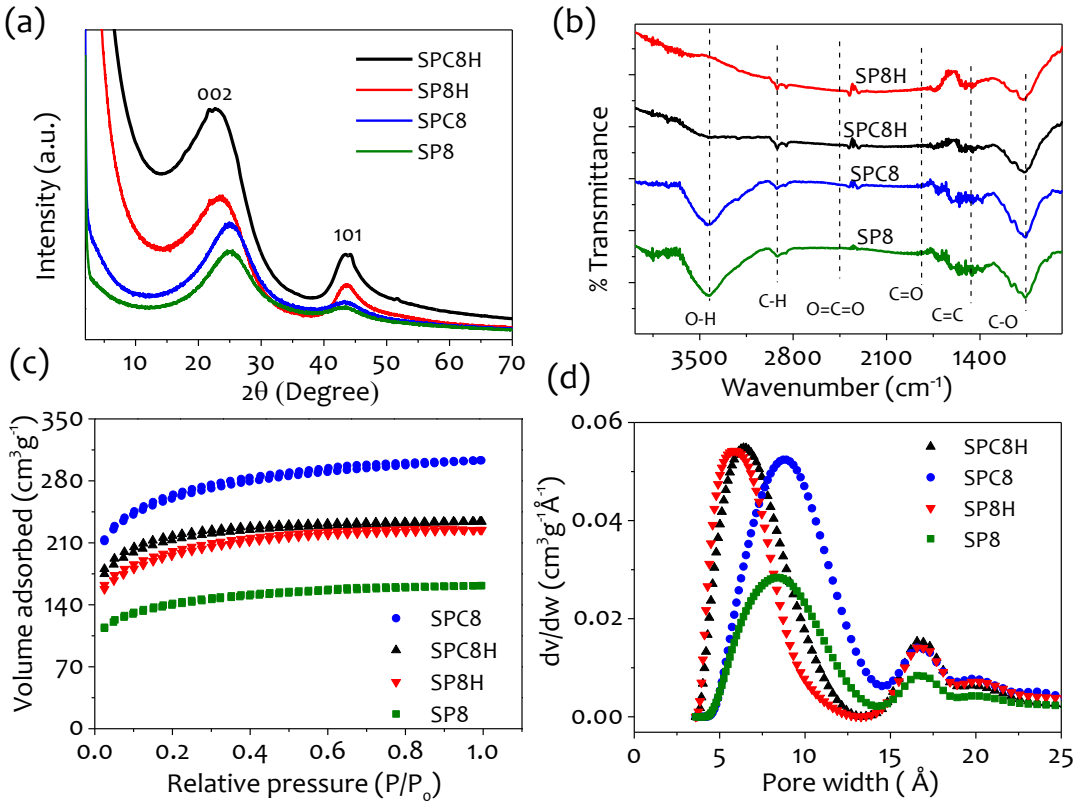

Figure 7.7: (a) X-ray diffraction (XRD) patterns, (b) Fourier-Transform Infrared Spectroscopy (FTIR) spectra and (c) BET isotherms for specific surface area (SSA) determination, and (d) NLDFT pore size distribution analysis of SPC8H, SP8H, SPC8, and SP8 carbon samples.

XRD scans were performed for SP8, SP8H, SPC8, and SPC8H carbon samples in the 2θ range of 2-70° (**Figure 7.7a**). The occurrence of 002 and 101 peaks in XRD patterns are characteristic of the presence of both amorphous and crystalline forms of carbon.[Bairi et al., 2016] The broad 002 peaks are associated with a high degree of disorder and hydrogen annealing results in the graphitic structure. On hydrogenation, there is an increase in the intensity of 101 peaks in comparison to the pyrolyzed carbon samples indicating the reorientation of the carbon atoms to form a crystalline graphitic structure. It is also observed that peak shifts in SP8H and SPC8H are towards the lower angles indicating the exfoliation of graphite. In Figure 7.7b, FTIR spectra show a wide band at 3500 cm^{-1} corresponding to -OH functional groups in case of pyrolyzed carbons (SP8 and SPC8), which disappears in hydrogen annealed carbon. Also, there is a slight decrease in the C=O and C-O bands on hydrogen annealing due to the surface passivation by -H, which in fact, is important for EDLC type behavior of supercapacitors.[Wang et al., 2013] BET adsorption isotherms and NLDFT pore size analysis in Figure 7.7c and d show the type-I curve with slight hysteresis indicating the presence of micro-pores of size below 2 nm in all the carbon samples. Interestingly, SPC8 carbon resulted in two times higher specific surface area (SSA = 828 m^2/g) as compared to that without catalyst (SP8, 434 m^2/g) that infers the role of catalyst in releasing the trapped gases, causing an increase in surface area and bringing in micro-porosity with an average size of 8.7 Å. It is observed that on hydrogenation, SSA of SPC8 decreased to 671 m^2/g (SPC8H), and pore size decreases to 6.3 Å, probably due to an increase in crystal size on graphitization. Surprisingly, the SSA of SP8 carbon increased on hydrogenation to 624 m^2/g (SP8H) due to the removal of sp^3 carbon leading to a high density of pores formation with a narrow size distribution, average pore size changing from 8.3 to 5.8 Å (Figure 7.7d). Interestingly, hydrogen annealing nullifies the differences in the surface effects while improvising the graphitization of SPC8H carbon.

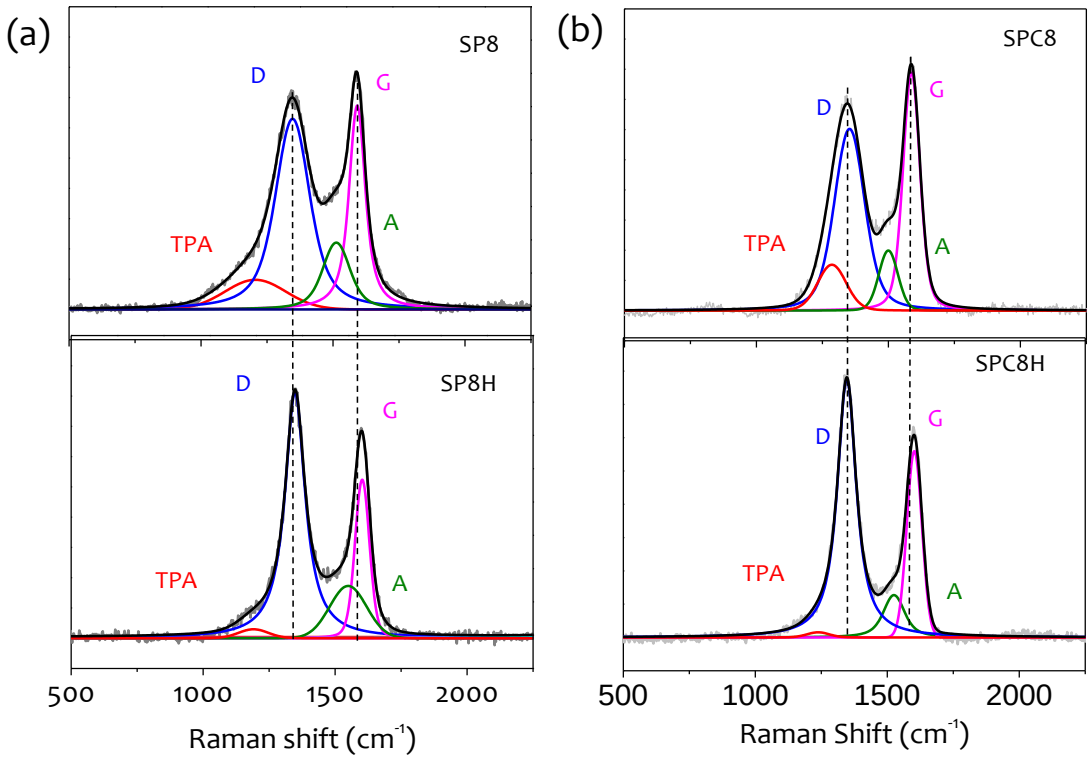

Figure 7.8: Deconvoluted Raman spectra of pyrolyzed carbon, before and after its hydrogenation (a) without catalyst (SP8 and SP8H) and (b) with a catalyst (SPC8 and SPC8H).

Deconvoluted Raman spectra of pyrolyzed carbon, before and after its hydrogenation (a) without catalyst (SP8 and SP8H) and (b) with a catalyst (SPC8 and SPC8H). Raman spectra of all the carbon samples are deconvoluted into four bands corresponding to different vibrational modes, as shown in **Figure 7.8** The occurrence of sharp G-band suggests graphitization, and D-band corresponds to the presence of defects sites. The I_D/I_G ratio was calculated and observed to be close to one for all samples indicating the formation of graphitic material (see Table 7.2). The defect band (D) is further deconvoluted in 2 bands. The broad peak around 1150 to 1200 cm^{-1} indicates the presence of alicyclic-aliphatic chains and transpolyacetylene-type (TPA) structures while a peak in-between the D and G-band represents the A-band corresponding to point vacancy defects.[Bokobza et al., 2015; Shi et al., 2017; Vázquez-Santos et al., 2012; Xing et al., 2017]

Table 7.1. Tabulation of parameters derived from Raman analysis.

Sample	Peak Position (cm^{-1})		FWHM (cm^{-1})		I_D/I_G	I_A/I_G
	D-band	G-band	D-band	G-band		
SPC8H	1348.89	1598.75	152.78	67.68	1.08	0.23
SPC8	1342.20	1589.64	202.33	75.89	0.96	0.25
SP8H	1348.89	1598.75	182.25	64.86	1.05	0.33
SP8	1342.20	1584.41	272.84	73.09	0.93	0.33

On hydrogen annealing, the pyrolyzed carbon with and without catalyst show a significant blue shift in the position of D-band (6.69 cm^{-1}) and in G-band (9.11 cm^{-1}), and there is a reduction in FWHMs as seen in Table 7.2 due to reduction in the defective graphenic domains. Moreover, the TPA-type structures appear in just-pyrolyzed carbon (SP8 and SPC8), the intensity of which reduces in SP8H and SPC8H carbon.

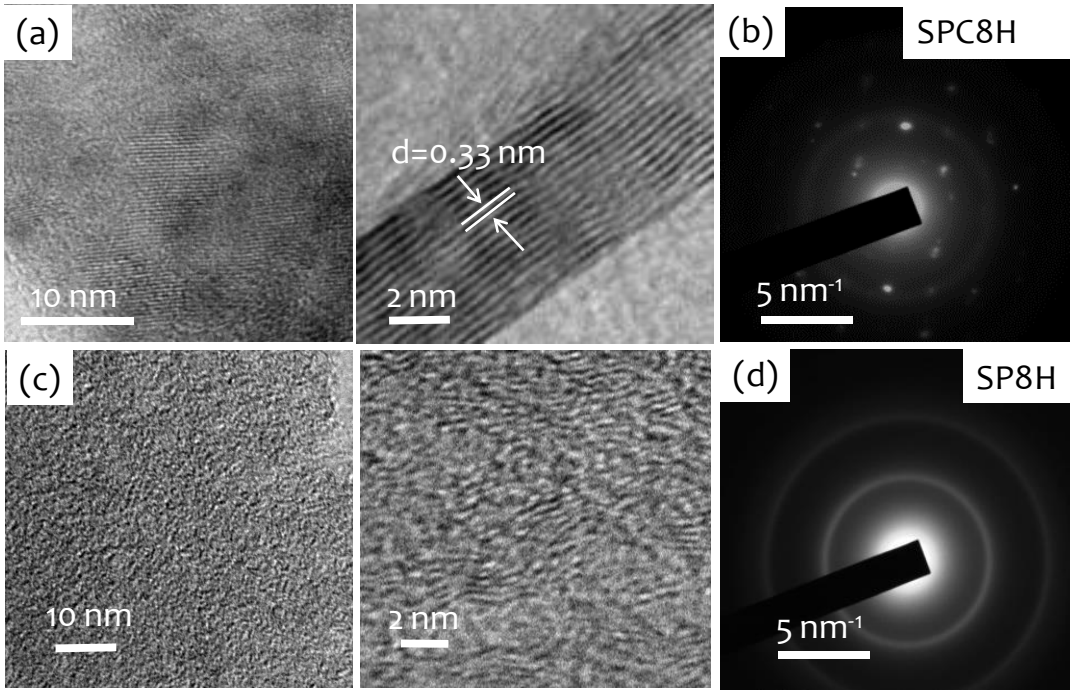

Figure 7.9: (a,c) HRTEM images along with the magnified view and (b,d) Selected Area Electron diffraction (SAED) pattern of SPC8H and SP8H, respectively.

In comparison to Figure 7.8a, the changes in Raman features, as discussed above, are more pronounced in Figure 7.8b due to the presence of a catalyst. In SPC8H carbon, there is a considerable amount of decrease in the point defects owing to the recrystallization of graphitic carbon in the presence of Ni catalyst. The I_A/I_G ratios were calculated to analyze the extent of local disorder in the carbon samples (Table 7.1). A significant decrease in the I_A/I_G is observed for the carbon samples prepared with Ni catalyst (SPC8H and SPC8) owing to a decrease in point defects. HRTEM images and SAED pattern from carbon samples before and after hydrogen annealing emphasizes the role of catalyst in graphitization (Figure 7.9). The SPC8H carbon clearly shows the appearance of discrete lattice planes with an interplanar spacing of 0.33 nm that corresponds to the 002 planes of the crystalline graphitic carbon (Figure 7.9b). However, no catalyst could be found after hydrogenation at 1000 °C The presence of sharp hexagonal spots in the ED pattern (Figure 7.9b) also confirms the sp^2 graphitization of carbon in the presence of Ni catalyst. The SP8H carbon obtained on pyrolysis without catalyst remains amorphous even after hydrogen annealing. As seen in Figure 7.9c, the absence of definite planes indicated sp^3 hybridized amorphous carbon. A diffuse ring in selected area electron diffraction in Figure 7.9d confirms that the amorphous phase is dominant in the absence of catalyst in SP8H carbon. Additionally, SPC8H carbon shows a remarkable improvement in the electrical conductivity due to an increase in sp^2 content on graphitization as compared to SPC8 carbon. As seen from the HRTEM images and ED patterns (Figure 7.10a), the SPC8 carbon on pyrolysis largely remains amorphous despite the presence of a catalyst. The presence of Ni nanoparticles could be detected in SPC8 carbon, as shown in Figure 7.10b. As calculated from the linear I-V characteristics (Figure 7.11a), SPC8H carbon posses ~two order higher electrical conductivity (53.03 S/m) than SPC8 (0.58 S/m).

7.4.3 Electrochemical Properties of the Graphitic Carbon

For analyzing the energy storage capability of these carbon materials, working electrodes were prepared by making a solution of graphitic carbon and Nafion binder followed by drop-casting it on glassy carbon electrodes for electrochemical characterization in three-electrode geometry (detailed in the experimental section).

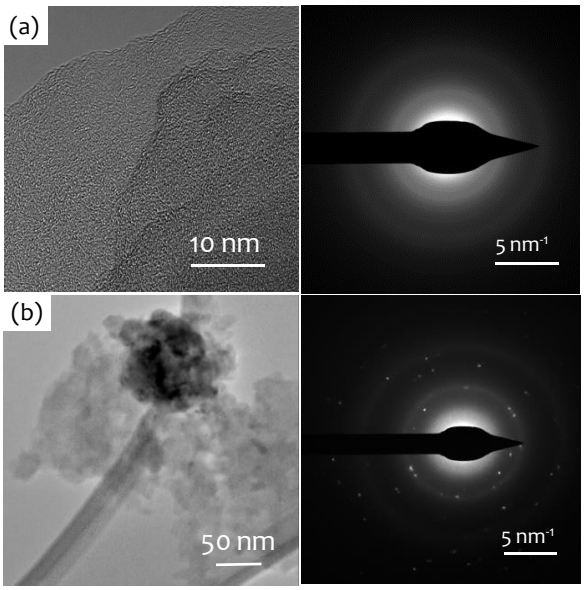

Figure 7.10: (a) HRTEM image and corresponding SAED pattern of SPC8 carbon. (b) Enlarged view of a Ni nanoparticle located in the sample and its corresponding ED pattern

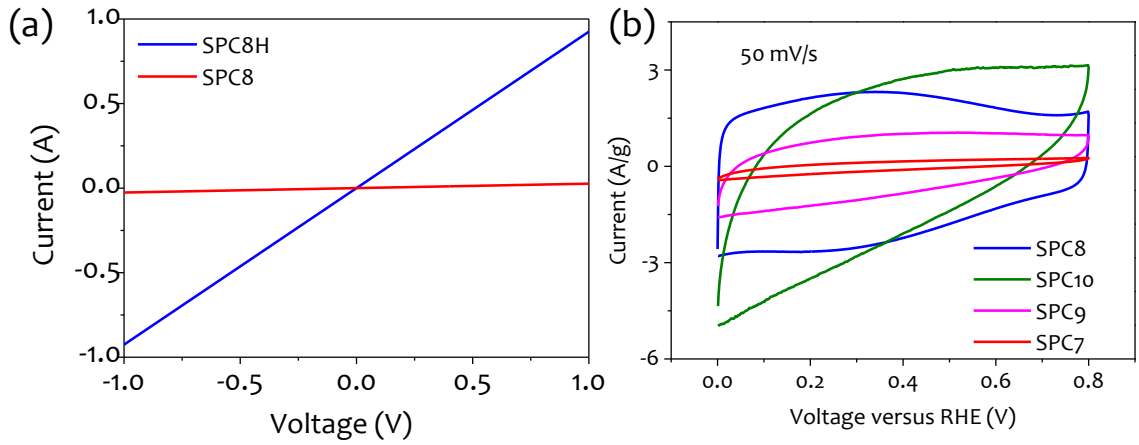

Figure 7.11: (a) I-V characteristics of SPC8H and SPC8 carbon. (b) Comparative CV curves of carbon material synthesized at different temperatures.

The CV curves of different carbon electrodes prepared at different carbonization temperatures and loading for optimization are shown in Figure 7.11b (see experimental section for details). The carbon pyrolyzed at 800 °C containing catalyst (SPC8) exhibited nearly rectangular CV scans compared to SP8 (Figure 7.12a) and SPC7, SPC9, SPC10 electrodes (Figure 7.11b) that exhibit leaf-like CV characteristics at 50 mV/s due to the non-graphitic and amorphous nature of the material. The carbon electrodes (SP8 and SPC8) exhibited a quasi-rectangular curve with low capacitance. Hydrogen annealed carbon (SPC8H), despite the reduction in SSA, exhibited ~2 times higher specific capacitance (145.3 F/g; calculated from CV) in comparison to SP8H and SPC8 due to significant improvement in crystallinity and graphitization (Figure 7.12a). The cyclic voltammograms of these carbon electrodes at different scan rates are shown in Figure 7.13. The values of current densities (J) at different scan rates (v) obtained at 0.4 V versus RHE for all the carbon samples are shown in Figure 7.12b. The data points were linearly fitted, and the R^2 values (goodness of linear fit) are plotted in Figure 7.12c. As observed in Figure 7.12c, R^2 approaches unity (~ 0.999) for SPC8H and deviates significantly for SPC8 and SP8H with a prominent deviation observed for SP8. The linearity in current density with scan rate confirms surface-controlled adsorption behavior, and any deviations from linearity with $(v)^{1/2}$ dependence are indicative of a diffusion-controlled process.

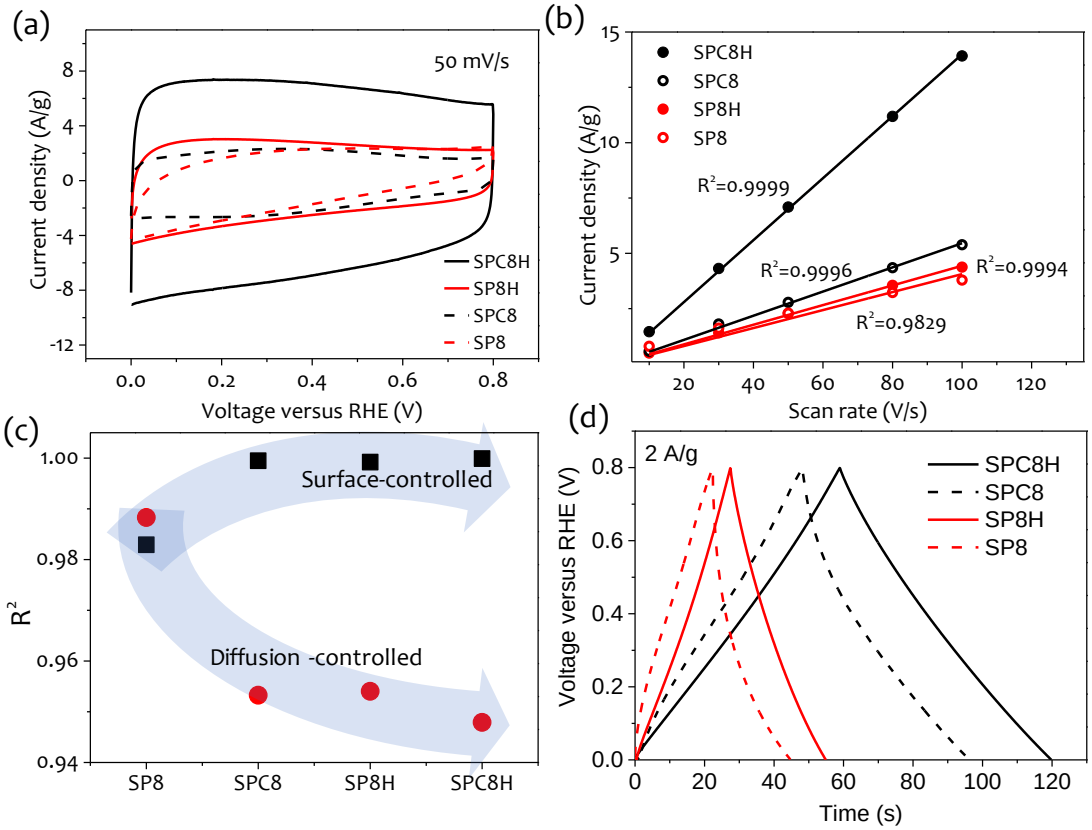

Figure 7.12: Comparative (a) cyclic voltammograms at a scan rate of 50 mV/s, (b) Current density (J) with respect to different scan rates at 0.4 V versus RHE, and (c) Goodness of fit (R^2) values for surface-controlled and diffusion-controlled process in SPC8H, SPC8, SP8H, and SP8 carbon electrodes. (d) Galvanostatic charge-discharge curves at 2 A/g of SPC8H, SPC8, SP8H, and SP8 carbon electrodes.

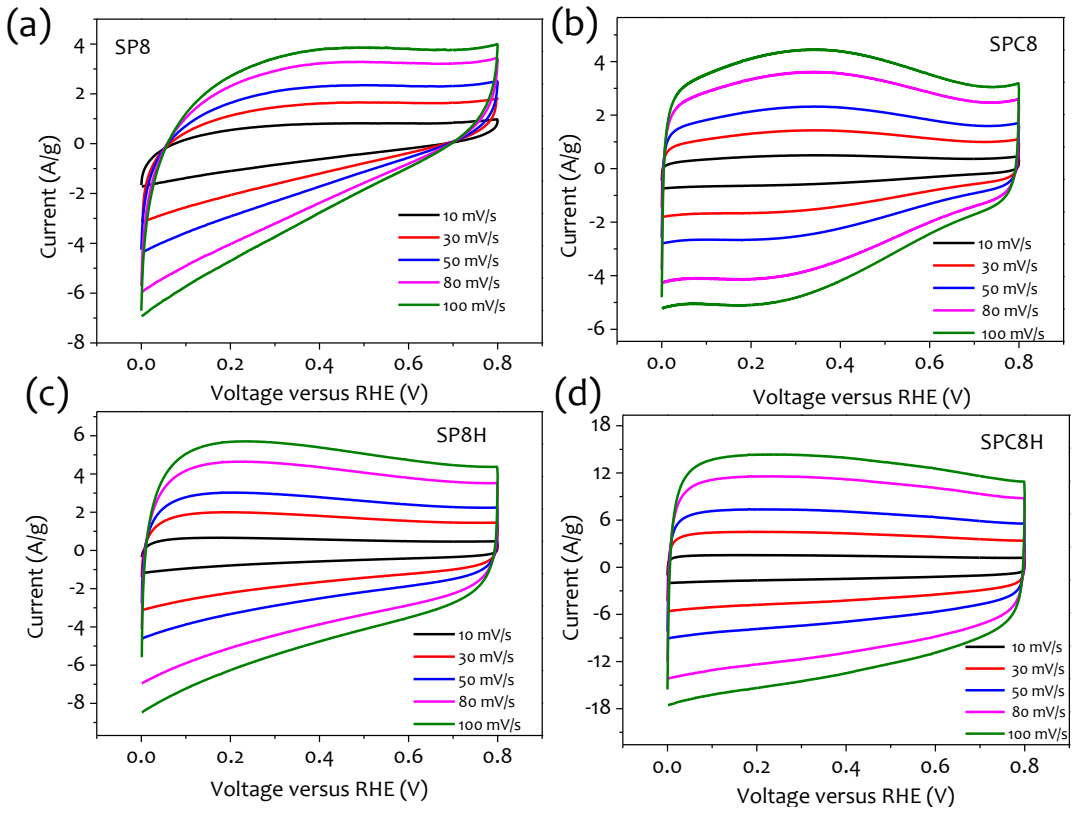

Figure 7.13: CV curves of (a) SP8, (b) SPC8, (c) SP8H, and (d) SPC8H carbon electrodes at different scan rates (10-100 mV/s).

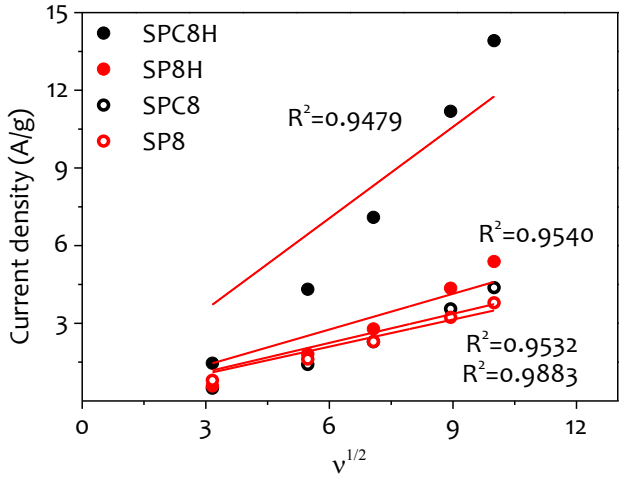

Figure 7.14: Current density at 0.4 V versus RHE as a function of square-root of scan rate $(v)^{1/2}$ for SPC8H, SPC8, SP8H, and SP8.

A reverse-trend is observed for linear dependence of J with $(v)^{1/2}$ with a maximum deviation of linearity for SPC8H and minimum for SP8 (Figure 7.14). This change-over in adsorption-mechanism is expected due to enhancement in graphitic crystallinity and reduction in surface functional groups upon hydrogen annealing for SPC8H and SP8H carbon electrodes.

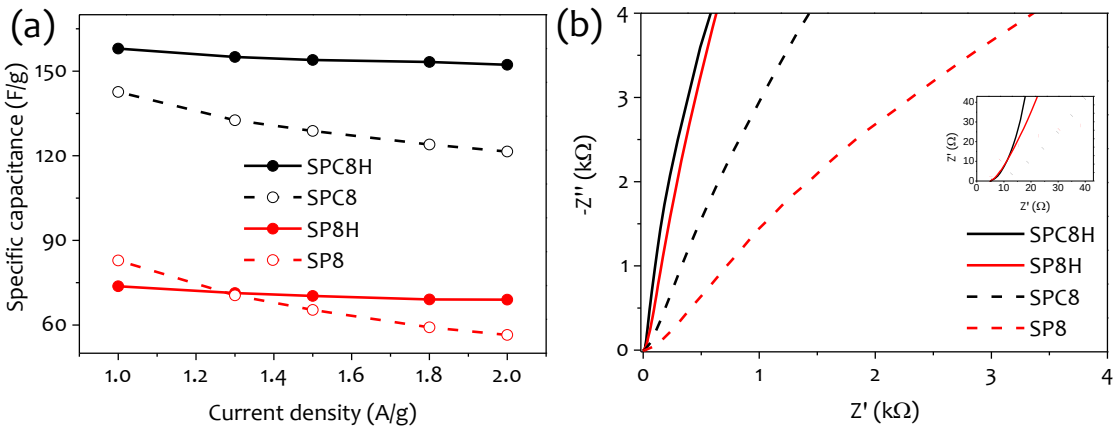

Figure 7.15: (a) variation in specific capacitance values at different current densities, (b) Nyquist plots (inset in b shows magnified Nyquist plot at high frequency) of SPC8H, SPC8, SP8H, and SP8 carbon electrodes.

In the galvanostatic charge-discharge measurements at an applied current density of 2 A/g, the carbon electrodes without catalyst (SP8 and SP8H) exhibited non-symmetric and skewed behavior with significant IR drop (Figure 7.15d). The pyrolyzed carbon with the catalyst (SPC8) based electrode shows a slightly better symmetric triangular curve that improves greatly in SPC8H with a higher area under the discharge curve indicating higher specific capacitance and negligible IR drop. Galvanostatic charge-discharge (GCD) measurements were performed in the range of 1-2 A/g, as shown in Figure 7.16, and the specific capacitance values were calculated from the plots, as shown in Figure 7.15a. SP8H and SPC8H exhibit excellent retention of capacitance (>95%) in the entire range of applied current density. SPC8H shows the highest specific capacitance of 158 F/g at 1 A/g (Figure 7.15a). The Nyquist plots give further mechanistic insight into the diffusion of ions and the ionic conductivity of the carbon electrodes (Figure 7.15b). The hydrogen annealed carbon samples exhibit significant improvement in the slope of the response curve in the low-frequency region due to an increase in the electronic conductivity.

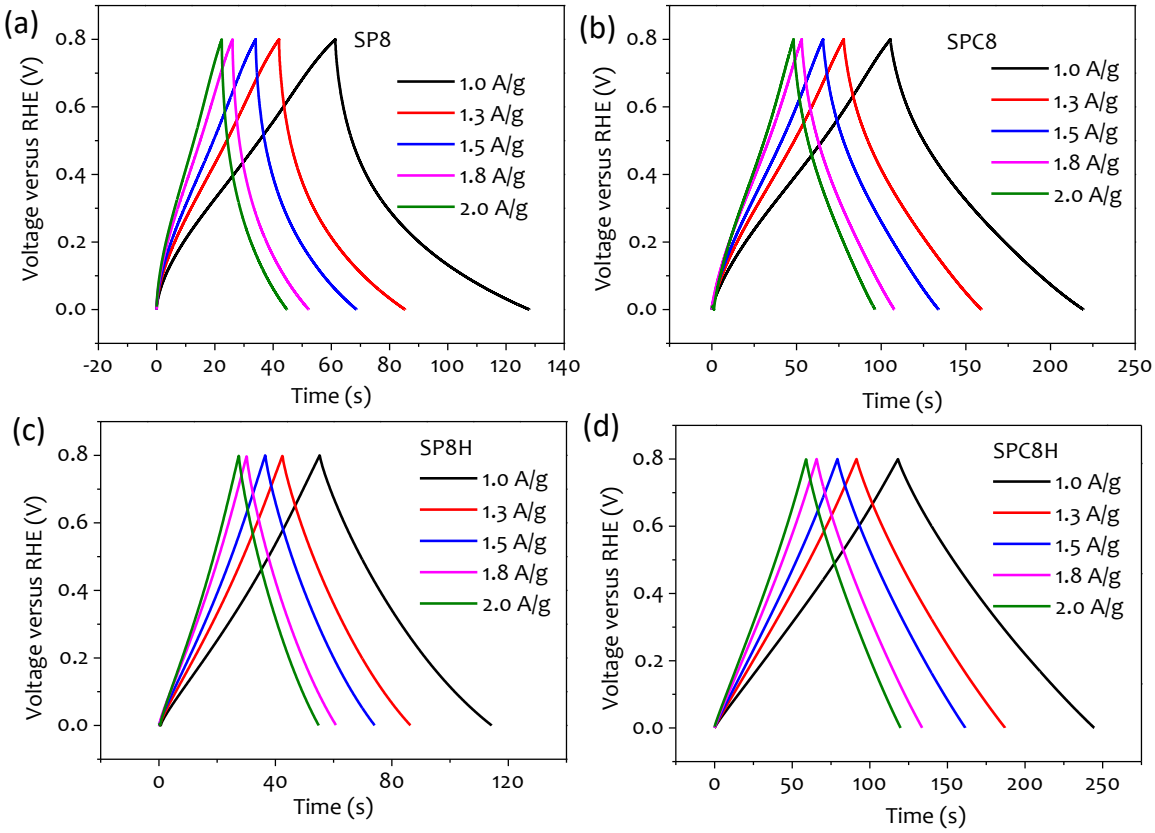

Figure 7.16: GCD curves of (a) SP8, (b) SPC8, (c) SP8H and (d) SPC8H carbon electrodes at different current densities (1-2 A/g).

SPC8H shows an excellent electric double layer capacitance (EDLC)-type supercapacitive behavior with an almost perpendicular linear part in low frequency and low resistance without any semicircle in high frequency (see inset Figure 7.15b). The SP8 and SPC8 samples are relatively more resistive, and thus deviate from the ideal capacitance behavior. The difference in the slope of SPC8 and SP8 obviously highlights the role of catalyst in improvising the conductivity during pyrolysis. In conclusion, the SPC8H exhibit enhanced supercapacitive performance due to the combined effect of increased graphitization and enhanced crystallinity, as observed in Raman and TEM analysis, respectively.

7.4.4 Energy Storage Performance of Graphitic Carbon Derived from Waste Polystyrene

Inspired by the excellent energy storage performance of the carbon material (SPC8H) prepared using the pristine polymer source, waste polystyrene (WP) plates were processed using the methodology as detailed in the experimental section and briefly presented in Figure 7.17a. The graphitic carbon obtained from waste polystyrene is abbreviated as SPC8H-WP and it exhibits electrochemical performance similar to that of SPC8H carbon derived from raw polystyrene in three-electrode geometry. Further, to demonstrate the application in the EDLC device, the measurements were performed in two-electrode Swagelok geometry using carbon cloth as a base electrode described in the experimental section. The device is abbreviated as SPC8H-WP/CC. The CV curves are almost rectangular, and current density increases with increasing scan rates (Figure 7.17b). Comparative CV curves at 10 mV/s of pristine carbon cloth (CC) and graphitic carbon on carbon cloth (SPC8H-WP/CC) are shown in Figure 7.18. Pristine CC supercapacitor device exhibit 2 order lower specific capacitance in comparison to SPC8H-WP/CC with a contribution of ~ 3% in the overall supercapacitive charge storage of the device.

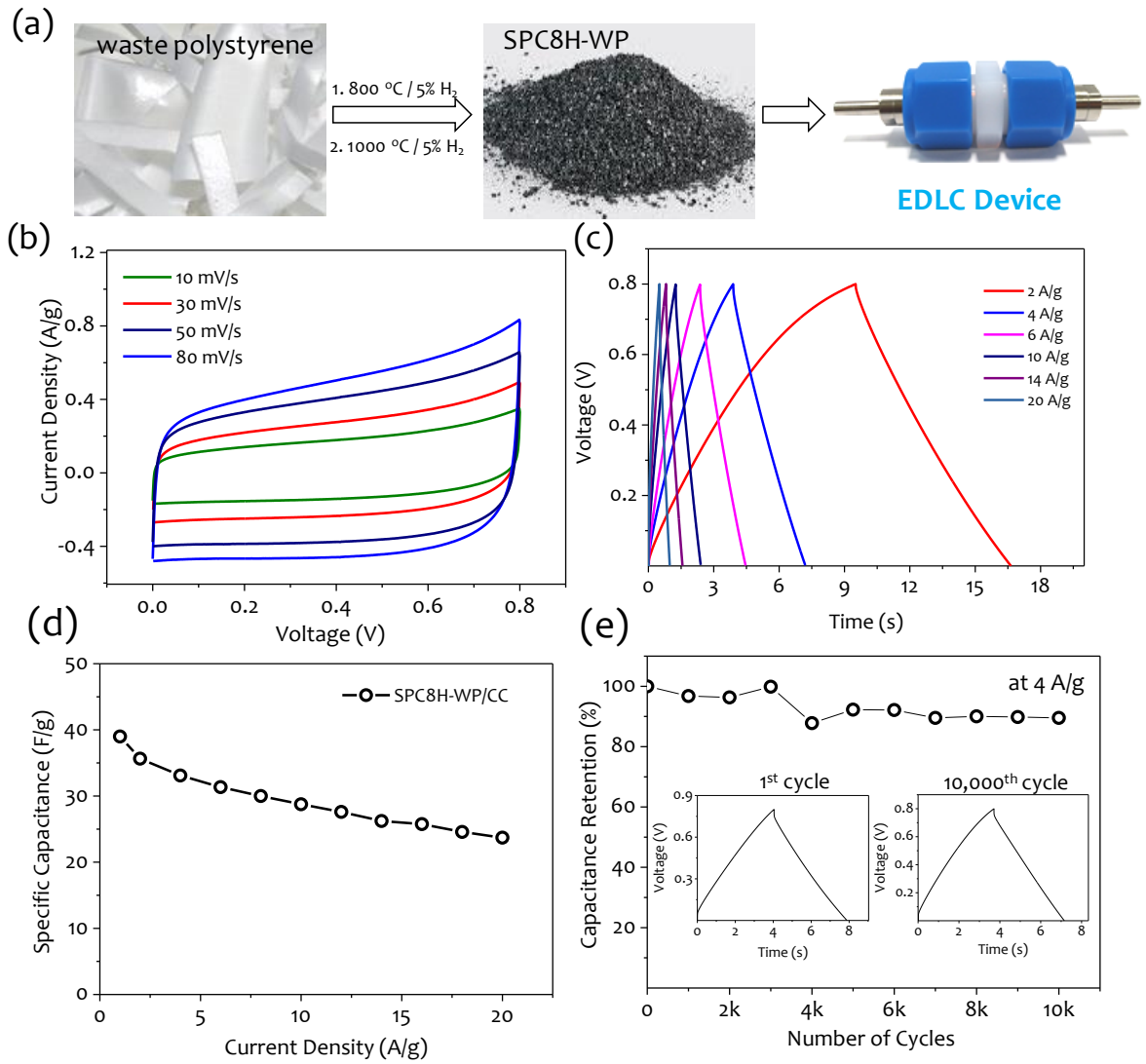

Figure 7.17: (a) Photograph of cut pieces of waste polystyrene plate used for converting to graphitic carbon for EDLC device fabrication. (b) CV at different scan rates, (c) GCD curves, (d) specific capacitance at different current densities, and (e) cyclic capacitance retention at 4 A/g for SPC8H-WP/CC carbon in two-electrode geometry. The insets show the 1st and 10,000th cycle of GCD measurement performed for the cyclic stability test.

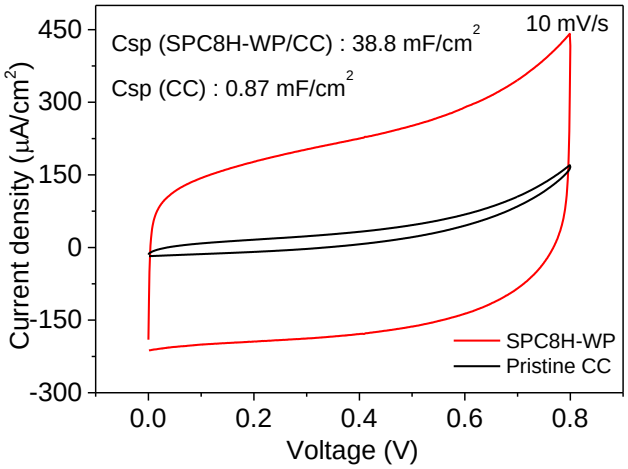

Figure 7.18: Comparative CV curves at 10 mV/s for pristine carbon cloth (CC) and graphitic carbon on carbon cloth (SPC8H-WP/CC) supercapacitor devices

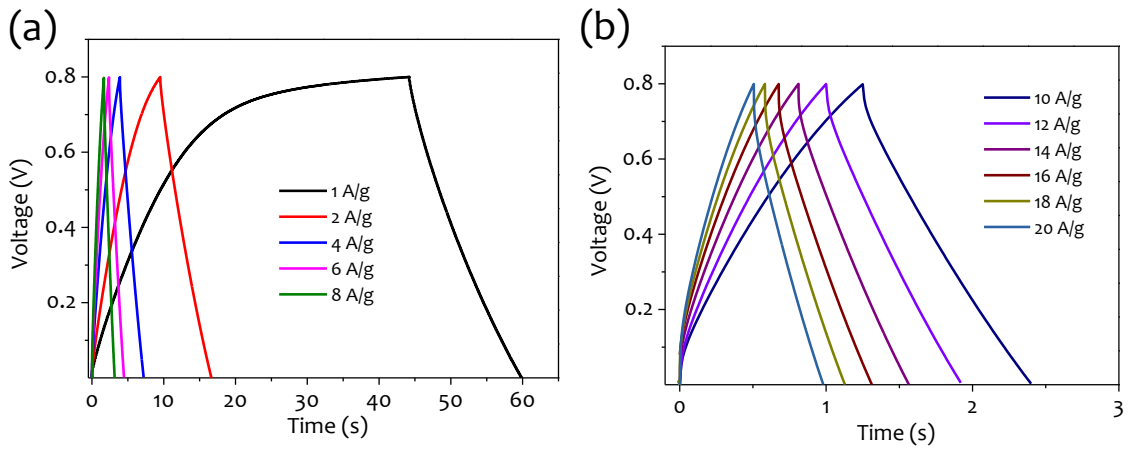

Figure 7.19: GCD plots for SPC8H-WP/CC at (a) low (1-8 A/g) and (b) high (10-20 A/g) current densities.

The GCD measurements in Figure 7.17c and Figure 7.19 exhibit nearly symmetrical triangular response with a small IR drop. The specific capacitance decreases gradually with increase in current densities and a highest specific capacitance of ~40 F/g is obtained at current density of 1 A/g (Figure 7.17d). For practical applicability, cyclic retention of capacitance is an important parameter. The fabricated device exhibit an energy density of ~ 0.8 Wh/kg with a corresponding power density of 198.7 W/kg, which decreases to ~ 0.52 Wh/kg at 3950 W/kg power density. The cyclic stability test was performed at a current density of 4 A/g for 10,000 cycles, as shown in Figure 7.17e Interestingly, the device exhibits higher stability with capacitance retention of ~90% after 10,000 cycles, which indicates the high operational stability of the device (insets, Figure 7.17e). The cyclic energy storage stability of waste polymer-derived carbon is commendable, and the slight decrease in specific capacitance with time could be due to gradual electrode deformation upon repeated cycling. Importantly, it may be noted that the specific capacitance values and cyclic stability of carbon derived from waste polystyrene are comparable to that of carbon derived from the pristine polymer sources and also from other waste polymer resources as observed in the literature (see, Table 1.5) Nevertheless, the energy storage capability and the quality of carbon material obtained from the waste plastic is of great significance. Thus, high surface area, good quality, conducting and crystalline carbon material has been derived from polystyrene-based plastic waste and explored as an excellent supercapacitive material.

7.5 Conclusions

In conclusion, a simple and low-cost method is demonstrated for the carbonization of waste polystyrene and sugar composite to give microporous carbon at 800 ^{o}C in 5% H_2 environment. A solution-processed Ni-butanethiolate complex is used as a catalyst for graphitization and improvement in the crystallinity of the carbon material. The processing conditions are systematically optimized for the formation of high-quality carbon with good conductivity, high specific surface area, and optimized pore geometry. The pyrolyzed carbon with a catalyst shows the highest surface area of 828 m^2/g. The carbon derived from waste polymer (SPC8H-WP) exhibits the specific capacitance of 120 F/g at 1 A/g. The two-electrode device fabricated using SPC8H-WP/CC carbon shows capacitance retention ~90% at 4 A/g over 10,000 cycles. The carbon produced can be used in sensing and water purification applications. This research work further advances the utilization of polystyrene and sugar-based waste carbon-rich products for industrial-scale synthesis of value-added carbon for various applications.